CARBON 50 (2012) 706–717

Available at www.sciencedirect.com

SciVerse ScienceDirect

journal homepage: www.elsevier.com/locate/carbon

Hard and tough carbon nanotube-reinforced zirconia-toughened alumina composites prepared by spark plasma sintering

J. Echeberria [a], N. Rodríguez [a], J. Vleugels [b], K. Vanmeensel [b], A. Reyes-Rojas [c], A. Garcia-Reyes [d], C. Domínguez-Rios [c], A. Aguilar-Elguézabal [c], M.H. Bocanegra-Bernal [c,*]

[a] CEIT and TECNUN (University of Navarra), 20018 San Sebastian, Spain

[b] Department of Metallurgy and Materials Engineering, Katholieke Universiteit Leuven, Leuven, Kasteelpark Arenberg 44, 3001 Heverlee, Belgium

[c] Centro de Investigación en Materiales Avanzados, CIMAV S.C., Laboratorio Nacional de Nanotecnologia, Miguel de Cervantes # 120, Complejo Industrial Chihuahua, Chihuahua 31109, Mexico

[d] Interceramic, Departamento de Investigación y Desarrollo, Av. Carlos Pacheco 7200, Chihuahua 31060, Mexico

ARTICLE INFO

Article history:
Received 12 July 2011
Accepted 14 September 2011
Available online 19 September 2011

ABSTRACT

It is demonstrated that 0.1 wt% of multi-walled carbon nanotubes (MWCNTs) or single-walled carbon nanotubes (SWCNTs) added to zirconia toughened alumina (ZTA) composites is enough to obtain high hardness and fracture toughness at indentation loads of 1, 5, and 10 kg. ZTA composites with 0.01 and 0.1 wt% of MWCNTs or SWCNTs were densified by spark plasma sintering (SPS) at 1520 °C resulting in a higher hardness and comparable fracture toughness to the ZTA matrix material. The observed toughening mechanisms include crack deflection, pullout of CNTs as well as bridged cracks leading to improved fracture toughness without evidence of transformation toughening of the ZrO_2 phase. Scanning electron microscopy showed that MWCNTs rupture by a sword-in-sheath mechanism in the tensile direction contributing to an additional increase in fracture toughness.

1. Introduction

Although the discovery of hollow and nanometer tubes composed of graphitic carbon has been attributed to Sumio Iijima [1], Rudushkevich and Lukyanovich [2] published clear images of 50 nm diameter tubes made of carbon and subsequently Oberlin et al. [3] showed hollow carbon fibres with nanometer-scale diameters using a vapor-growth technique and Abrahamson et al. [4] reported evidence of carbon nanotubes at the 14th Biennial Conference of Carbon at Penn State University [5]. The combination of small size, low density, large aspect ratio of the carbon nanotubes, commonly abbreviated as CNTs, either single-walled (SWCNT) or multi-walled (MWCNT), with their outstanding mechanical properties should be ideal reinforcing/functionalizing elements for composites. The mechanical and physical properties depend in great measure of factors as synthesis method and defects introduced during nanotube purification [6]. The combination of impairments introduced during sample preparation as well as inadequate measurements has lead to obtain a variety of nanotube tensile strengths [7]. Reports on mechanical properties described in the open literature, are all focused on multi-walled carbon nanotubes obtaining lower values for fracture strengths and failure strains. For example, Yu et al. [8] reported mean fracture strength of 28 GPa in arc-discharge-grown MWCNTs, failure strains ranging from 2 to 13%, tensile strength of ~11–63 GPa and a modulus values between 270 and 950 GPa. Meanwhile, Barber et al. [7] demonstrated

* *Corresponding author:* Fax: +52 614439 4852.
E-mail address: miguel.bocanegra@cimav.edu.mx (M.H. Bocanegra-Bernal).
0008-6223/$ - see front matter
doi:10.1016/j.carbon.2011.09.031

multishell failure at low failure strains (approximately 5%) in multi wall carbon nanotubes produced by chemical vapor deposition (CVD). The experimental results by Peng et al. [6], displayed strengths around of 100 GPa and fracture strains close to theoretical predictions. Yamamoto et al. [9] obtained tensile strengths ranging from 2 to 48 GPa (mean 20 GPa) in 10 pristine MWCNTs while for 10 acid-treated MWCNTs with channel-like defects, the tensile strengths were 70% lower than those of the pristine MWCNTs (~1–18 GPa, mean 6 GPa). As already noted, catalytically produced MWCNTs are much less perfect in structure than arc grown tubes, and are therefore considerably less stiff. CNTs defects-free could reach a Young's moduli in the order of 1 TPa, high failure strains (~15–30%), and tensile strength higher than 100 GPa [10,11].

Nowadays, research is devoted to the possible incorporation of CNTs in a polymer [12], metal [13,14], or ceramic [15,16] matrix in order to improve the performances of these materials [17,18]. In particular, the extreme brittle nature of ceramics restricted them from numerous advanced structural applications and therefore, the addition of CNTs to ceramic matrix composites has been conducted to improve their fracture toughness [19,20]. Although the role of CNTs in the sintering of ceramic composites is not completely clarified in literature, some interesting work has been performed. For example, An et al. [21] studied the influence of the CNT content on the tribological properties of CNT/Al_2O_3 composites and reported a 30% increase in microhardness compared to pure Al_2O_3; Siegel et al. [22] reported a 24% increase in fracture toughness of alumina with additions of 10 vol% MWCNTs. More recently, Zhan et al. [15] prepared 100% dense Al_2O_3 + 10 - vol% SWCNTs at 1150 °C during 3 min using spark plasma sintering (SPS) resulting in a fracture toughness of 9.7 MPa $m^{1/2}$ being nearly three times that of nanocrystalline alumina, but the results have not been reproduced up to now.

Wang et al. [23] prepared alumina reinforced with 10 vol% SWCNT using the SPS technique obtaining a fracture toughness for SWCNT/alumina similar to that of graphite/alumina applying the single-edge notched beam (SENB) technique suggesting a poor connectivity between the SWCNTs and alumina matrix. Until now, very little or no improvements with respect to toughening were reported in CNT reinforced ceramics [17]. Generally, the negative effects of the additions of CNTs could be imputed to problems such as inhomogeneous dispersion in the ceramic matrix caused by agglomeration of carbon nanotubes which in turn can be resources of cracks.

Alumina based composites represent a new generation of ceramic materials as an alternative to biomedical-grade alumina and zirconia and the most promising candidates for replacing metallic bearing parts in arthroplastic applications [24] requiring an important control of the resulting microstructure, superior and reliable mechanical properties as well as high bio-inertness and biocompatibility [25]. Zirconia toughened alumina (ZTA) composites have many applications in which wear resistance and mechanical strength are required. To improve their mechanical properties, sintering by hot-pressing (HP) and hot isostatic pressing (HIP) are frequently used [26]. The use of HIP in ceramic composites for biomedical applications minimizes the residual stresses within ceramic pieces and gives composites with a density close to the theoretical one, improving both strength and reliability of the product [27]. HP on the other hand is limited to the formation of simple geometries and moderate sizes. A comparatively new sintering process at low temperature with short holding time, denominated spark plasma sintering (SPS), also commonly known as pulsed electric current sintering (PECS), has been directed towards the development of metallic materials, structural ceramics, oxide superconductors, ceramic composites and functionally graded materials [28,29].

SPS has been demonstrated to enable the consolidation of ceramic materials within minutes avoiding exposing the powder compacts to high temperatures for a long duration. Taking into account that SPS has been used as mentioned above to produce metal and engineering ceramics, there are few reports on the application of this technique to produce dense ceramics for different biomedical applications.

Although the main part of the reported SPS applications are still in the area of material development, several opportunities for industrial implementation have been generated [30] in order to realize a manufacturing process with optimum cost efficiency. Current developments are related to the industrial production of more complex geometries as well as further optimization of quality and costs [31–36]. In the present work, we developed ZTA composites with an optimized amount of SWCNT or MWCNT additions showing a combination of high hardness (~22 GPa) and high fracture toughness (up to 8.2 MPa $m^{1/2}$). Although MWCNTs can be considered to be less efficient concerning a mechanical reinforcement, SWCNTs form aggregates of bonded and aligned CNT bundles which are difficult to separate and infiltrate with the matrix affecting notably the mechanical properties as was demonstrated by Bocanegra et al. [37] who found that the fracture toughness of pressureless sintered MWCNT-reinforced ZTA was 41% higher than for the ZTA matrix material and 44% higher than for the SWCNTs reinforced equivalent. This appreciation can also be supported with results by Yamamoto et al. [38] in MWCNT/Al_2O_3 composites. In this context, the present investigation is taken up to study in depth the densification and mechanical properties of MWCNT and SWCNT reinforced zirconia toughened alumina composites using SPS as a processing tool. Taking advantage of the electrical conductivity and chemistry of carbon nanotubes, these composites could find applications in smart multifunctional orthopaedic implants with the capacity for monitoring implant interactions with extracellular matrix components. Besides this, lower concentrations of carbon nanotubes and higher purity have shown to reduce notably the cytotoxicity towards T lymphocytes [39]. Following this, the lower amounts of SWCNT and MWCNT added to our ZTA composites will enable more complicated designs and shapes and will open the door to several applications in the field of orthopaedic implants considering that with low ZrO_2 additions to the composite, aging by low temperature degradation could be reduced or avoided.

2. Experimental procedure

2.1. Starting materials

High purity Baikalox SM8 Al_2O_3 (>99.99, 100% α), ZrO_2 + 3 mol% Y_2O_3 (thereafter abbreviated as TZ-3Y), monoclinic ZrO_2 and

MgO were used as starting powders. Their characteristics provided by the suppliers (particle size, surface area and theoretical density) are presented in Table 1. MWCNTs (Catalysis Laboratory of CIMAV S.C. [40]), diameter 70–110 nm, length 120–160 μm, purity >95%, surface area 25 $m^2 g^{-1}$, and high purity SWCNTs (HELIX Material Solutions), diameter ~1.3 nm, length 0.5–40 μm, purity >90%, and surface area >300 $m^2 g^{-1}$ were used as reinforcement.

2.2. Mixing procedure

Homogeneous mixtures of Al_2O_3 + 0.025 wt% MgO + 13 wt% TZ-3Y + 2 wt% $ZrO_{2(m)}$ (thereafter abbreviated as C2) with additions of 0.01 and 0.1 wt% of MWCNTs or SWCNTs were prepared. A composite without additions of CNTs was also prepared for comparison. The as-received MWCNTs and SWCNTs were carefully dispersed in 500 mL ethanol with an ultrasonic probe for about 2 h. The nanopowders and the dispersed MWCNTs or SWCNTs alcohol media were vigorously stirred with a 5 × 1 cm magnetic bar at 40 °C until most of the ethanol had evaporated and subsequently the mixture was dried at 100 °C for 12 h. Finally, the agglomerated powder mixture was judiciously ground in an agate mortar.

2.3. Sintering procedure

Sintering experiments were performed on a FCT FAST device (Type HP D 25/1, FCT Systeme, Rauenstein, Germany), which is a Spark Plasma Sintering (SPS) furnace equipped with a 250 kN uniaxial press. The process chamber can be evacuated down to 0.05 Pa. The power supply can provide a pulsed DC up to 8000 A at a voltage up to 10 V through the electrodes to the tool set-up that contains the specimen. Conical graphite protection plates are placed between the punches and the water cooled electrodes (Fig. 1). A pulsed as well as a constant DC with on/off cycles of 0–255 ms (on-time)/0–255 ms (off-time) can be generated. A pulse–pause combination of 10–5 ms was used throughout all the experiments. A preset time–temperature profile is generated by controlling the power, which is done by controlling the voltage difference over the electrodes. In this way, the current flowing through the specimen-punch-die set-up is controlled.

A 30 mm diameter graphite die (FE 779 grade, Schunk, Germany) with a die wall thickness of 8.5 mm was used, while 5 mm thick samples were prepared. In order to minimize the radiation heat losses from the die wall, it was surrounded by 10 mm thick porous carbon felt. During the experiments, the temperature was measured by a central pyrometer with a focus point at the bottom of the central borehole inside the upper punch, 5 mm from the top of the powder compact (Fig. 1). SPS experiments were performed at 1520 °C, applying a heating rate of 100 °C/min. The pressure was gradually increased from 7 to 40 MPa during the heating stage, while a maximum pressure of 80 MPa was applied at the sintering temperature. The density was measured by means of a Quantachrome Multipycnometer (by Quantachrome Instruments, USA) using Helium as displacement gas for the as-sintered composites. The surfaces of the obtained samples were ground on a diamond wheel and polished by SiC paper

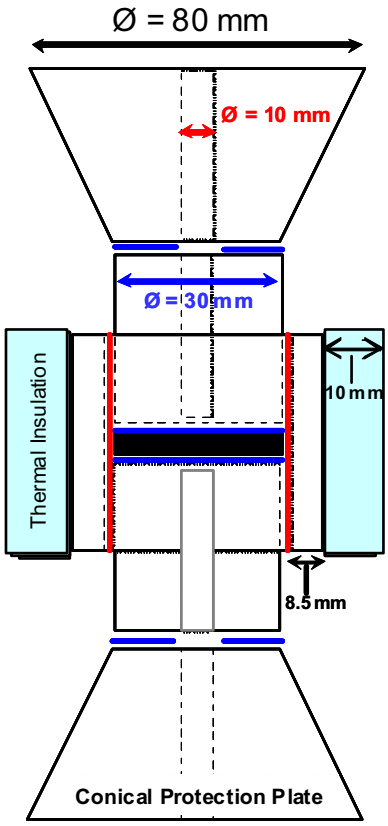

Fig. 1 – Schematical representation of the PECS sinter set-up used for densification of the zirconia toughened alumina (ZTA) composites reinforced with MWCNTs and SWCNTs. A 30 mm graphite die with a die wall thickness of 8.5 mm was used. Porous carbon felt insulation was used to reduce the radiation heat losses from the graphite die wall.

Table 1 – Characteristics of commercial starting powders.

Powder	Primary particle size (μm)	BET surface area ($m^2 g^{-1}$)	Theoretical density ($g cm^{-3}$)
Baikalox SM8 Al_2O_3[a]	0.050	10.0	3.98
3 mol% Y_2O_3–ZrO_2 (TZ-3Y TOSOH)[b]	0.075	17.2	6.05
MgO 500A[c]	0.053	31.9	3.58
Monoclinic ZrO_2[d]	<50 nm	15–35	5.89

[a] Supplied by Baikowski (USA).
[b] Supplied by TOSOH (Japan).
[c] Supplied by UBE Chemical Industries (Japan).
[d] Supplied by Sigma Aldrich (USA).

and polished to a mirror finish by diamond pastes of both 0.5 and 0.25 μm. Samples were thermally etched at 1370 °C for 30 min, following the procedure described elsewhere [37].

2.4. *Characterization*

The polished and fracture surfaces were characterized by scanning electron microscopy (SEM: JEOL JSM 5800 LV, Japan, and FEG SEM: JEOL JMS 7000F, Tokyo, Japan) using an accelerating voltage of 2 kV. The average grain size in pure ZTA (C2), C2 + 0.01 wt% MWCNTs or SWCNTs, and C2 + 0.1 wt% MWCNTs or SWCNTs composites was measured using the linear intercept technique using 400–500 grains for each sample. In order to study the preservation of the carbon nanotube structure at the sintering temperature, Raman spectra were obtained with a Thermo Nicolet Almega XR Dispersive Raman Spectrometer (λ_{ex} = 532 nm and maximum power 20 mW).

2.5. *Mechanical properties*

Vickers hardness measurements were carried out on sintered samples using a microhardness tester FM-7 (Future-Tech, Tokyo, Japan). Approximately 10–20 indents per ceramic grade were made on polished surfaces applying a load of 1, 5, and 10 kg held for 15 s and an average hardness was determined. The separation between neighboring indentations was more than four diagonal lengths of the indentation impression following the standard ASTM C1327-99 for Vickers indentation hardness of advanced ceramics [41]. The corresponding indentation sizes and crack lengths were measured with the help of an optical microscope Olympus PMG3 (by Olympus Co., Japan) soon after indentation to prevent the slow crack growth associated with the stress field that acts after removal of the indenter and the environment. The indentation fracture toughness (K_{IC}) was derived from the average crack length. For a ratio $c/a > 2.5$ (present study), where c is the crack length and a the half diagonal length of the indentation impression, K_{IC} was calculated using the equation derived by Evans and Charles [42].

3. Results and discussion

The sintered MWCNT and SWCNT reinforced zirconia toughened alumina composites exhibited relative densities higher than 98% as can be seen in Fig. 2. On the whole, the relative density decreases as the fraction of CNTs increases, but the ones with MWCNTs always had higher densities than the ones with additions of SWCNTs. From this Fig. 2 it is clear that the minimum density corresponds to ZTA composites with 0.1 wt% of SWCNTs which could be associated to the presence of CNT agglomerates, their dispersion in the matrix is difficult resulting in a lower sintered densities [43]. In fact, the density reduction of the ceramic composites with increasing amount of carbon nanotubes content in the matrix is a well-documented phenomenon [44,45]. Nevertheless, even if the carbon nanotubes are well-dispersed, their addition can have adverse effects on the sintering kinetics [45]. Intuitively, one would the density expect to decrease with increasing CNT addition from 100% TD for the ZTA to a lower absolute density due to the internal porosity that is intrinsically linked to CNTs

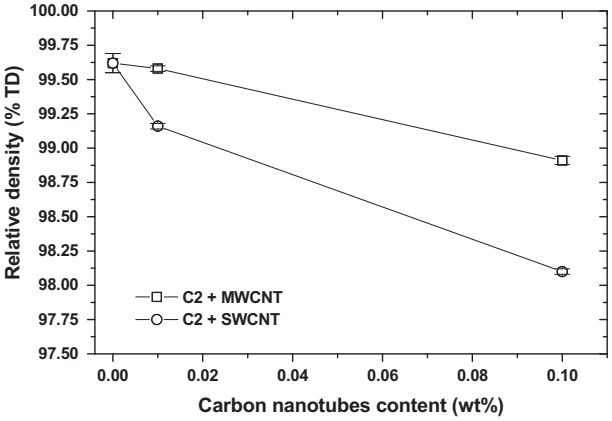

Fig. 2 – Relative density (% TD) as a function of carbon nanotubes content (wt%).

that are embedded in a dense matrix (the internal pore channel of the CNT should be reflected as a lower density of the composite). The theoretical density of CNT's only concerns the carbon sheets and does not take into account the internal pore channel, which is present and contributes effectively to a lower overall density of the composite.

The polished and thermally etched surfaces of pure ZTA (Fig. 3a) and ZTA composites containing 0.01 wt% MWCNTs and SWCNTs (Fig. 3b and c, respectively) and 0.1 wt% MWCNTs and SWCNTs (Fig. 3d and e, respectively), all SPSed at 1520 °C, are compared in Fig. 3. As shown in the micrographs, all samples were crack-free with submicrometer sized equiaxed grains. A lower magnification of the dense samples shown in the Fig. 3a–e is presented in Fig. S1 in Supplementary material. The mean Al_2O_3 and ZrO_2 grain size in the CNT free composites was 0.86 ± 0.37 and 0.29 ± 0.12 μm respectively, while for the composites with additions of 0.01 wt% MWCNTs and SWCNTs and 0.1 wt% MWCNTs and SWCNTs, the mean Al_2O_3 grain size was 0.73 ± 0.32, 0.68 ± 0.28, 0.68 ± 0.28 and 0.78 ± 0.33 μm respectively, whereas the ZrO_2 grain size was respectively 0.25 ± 0.09, 0.24 ± 0.09, 0.30 ± 0.11 and 0.32 ± 0.14 μm, as summarized in Table 2, which in turn confirms that the reduction in grain size can be attributed to grain pinning by the presence of CNTs. CNTs have a greater effect on the grain size retardation mechanism and dimensionalities of the CNTs because they are mainly located at the grain boundaries forming a strong entangled network preventing the grains closing during densification and offering fine grains in the final composite by grain pinning [16,45]. The grain growth is observed to decrease with increasing CNT content.

On the other hand, it is important to point out that the presence of zirconia particles (white spots phase) slows down the movement of the grain boundaries of alumina so that the grain size of the alumina matrix is decreased [46]. The local absence of zirconia particles located at the grain boundaries induces alumina grain growth as can be seen in Fig. 3c. Table 2 summarizes the sintered densities and mean grain sizes of alumina, zirconia of each composite.

The Vickers hardness of MWCNT and SWCNT reinforced ZTA composites is compared with pure ZTA sintered under the same SPS treatment conditions in Fig. 4 as a function of

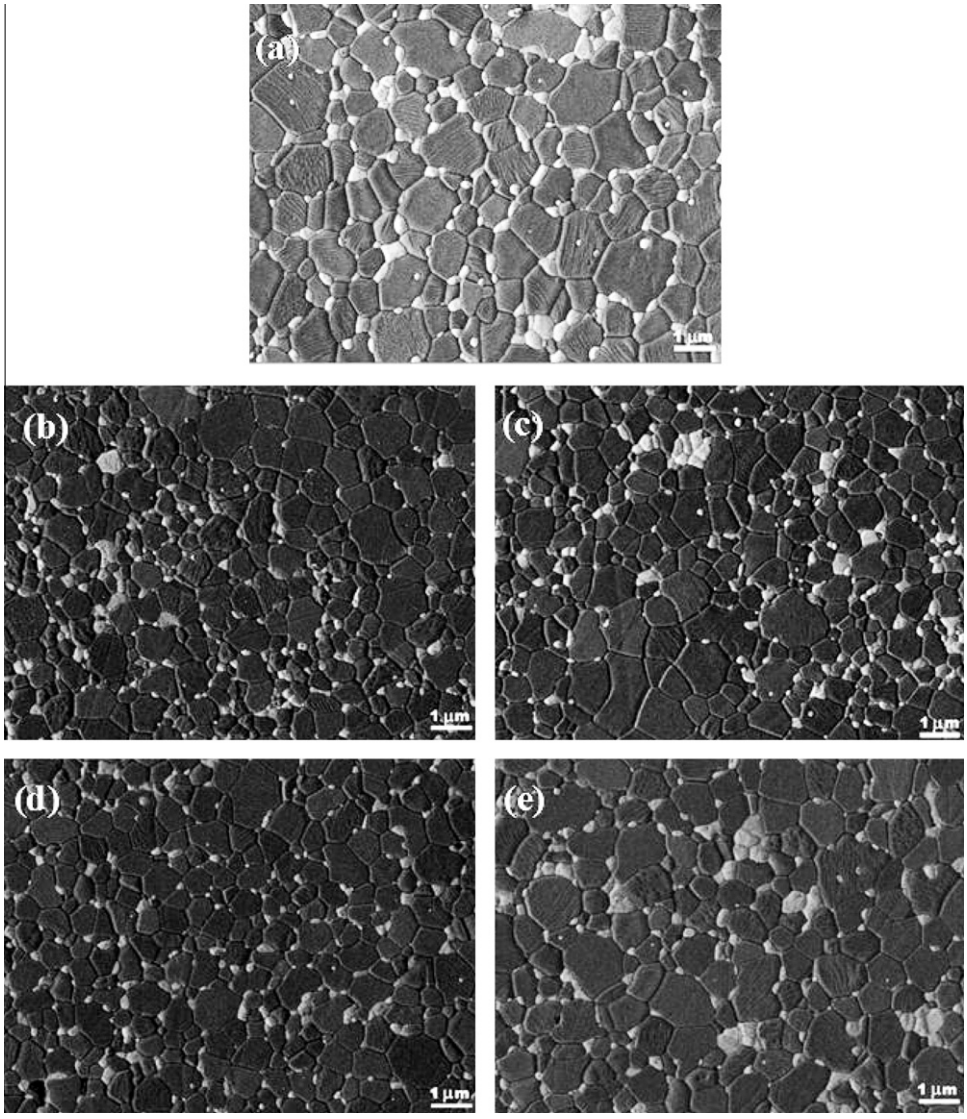

Fig. 3 – Typical SEM micrographs of polished and thermally etched surfaces of as-SPSed (a) pure ZTA (C2), (b) C2 + 0.01 wt% MWCNTs, (c) C2 + 0.01 wt% SWCNTs, (d) C2 + 0.1 wt% MWCNTs, and (e) C2 + 0.1 wt% SWCNTs composites SPSed at 1520 °C.

Table 2 – Relative density and measured grain sizes for the experimented composites.

Sample	Relative density (% TD)	Grain size Al_2O_3 (μm)	Grain size ZrO_2 (μm)
C2*	99.62 ± 0.07	0.86 ± 0.37	0.29 ± 0.12
C2MW0.1	98.91 ± 0.03	0.68 ± 0.28	0.30 ± 0.11
C2SW0.1	98.10 ± 0.02	0.78 ± 0.33	0.32 ± 0.14
C2MW0.01	99.58 ± 0.02	0.73 ± 0.32	0.25 ± 0.09
C2SW0.01	99.16 ± 0.02	0.68 ± 0.28	0.24 ± 0.09

* C2: Al_2O_3 + 0.025 wt% MgO + 13 wt% ZrO_2 (Tosoh 3Y) + 2 wt% $ZrO_{2(m)}$.

the indentation load. The hardness results reflect the influence of two microstructural parameters, the indentation load as well as the CNT content. A clear decrease in hardness up to 5 kg indentation load is observed, after which the hardness tends to level off. Higher hardness values result in improved wear and scratch resistance which in turn is a favorable condition for applications in orthopaedic implants, although it generates additional difficulties during final machining. For all indentation loads, the composites with additions of 0.1 wt% MWCNTs reached a maximum hardness, while composites with additions of 0.1 wt% SWCNTs exhibited an even lower hardness values compared to the pure ZTA, suggesting an agglomeration of the SWCNTs. This behavior is in good agreement with the report by Zhang et al. [47]. As pointed out by Correa de Sá e Benevides de Moraes et al. [48], the indentation load affects the indentation size and the crack

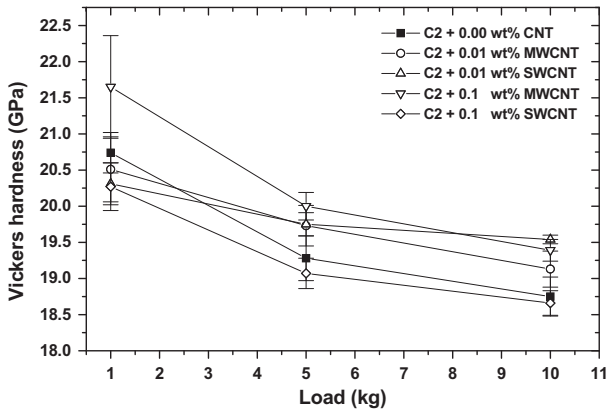

Fig. 4 – Plot of the Vickers hardness as a function of indentation load for ZTA composites with and without additions of CNTs.

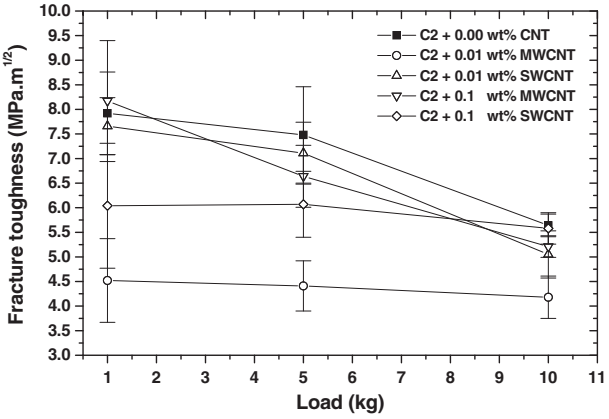

Fig. 5 – Plot of the fracture toughness as a function of indentation load for ZTA composites with and without additions of CNTs.

length, being both dependent on the sample dimension and microstructure of the material. However, most ceramic composites show a hardness decrease with increasing load, known as the indentation size effect (ISE) [49,50].

It is observed that the scatter and standard deviation on the measurements decreases with increasing indentation load, making the reported data also more statistically reliable. Our results are in agreement with these observations, as shown in Fig. 4. Although there is a well-known dependency of hardness on load, a full characterization by hardness-load relationships is rather uncommon for ceramics [51]. It can be asserted that the toughness values obtained by the indentation technique in structural ceramics are fundamentally different from the fracture toughness K_{IC} obtained by conventional method and therefore, have some drawbacks. The validity of the IF technique to determine K_{IC} of CTN-ceramic composites has been specifically questioned in the literature [52]. In spite of this, indentation fracture can be used to rank CNT composites effectively, for well densified material (sintered densities greater 98%) with a good nanoscale dispersion [53], taking into account that all the models employed in the K_{IC} calculations are essentially based on the same parameters and the differences are related to equation coefficients. Nevertheless, in many cases, these coefficients have been determined considering experimental studies in which K_{IC} has been compared with measurements carried out by conventional procedures [54].

The variation of the fracture toughness, K_{IC}, calculated from the Vickers indentation crack size measurements at different loads is illustrated in Fig. 5. The fracture toughness for each composition slightly varies as a function of the indentation load. It is noteworthy that for the composites with a coarser microstructure (ZTA without addition of carbon nanotubes, Table 2) the fracture toughness is relatively higher as compared to the composites doped with both SWCNTs and MWCNTs for all indentation loads. On the other hand, when fracture toughness is plotted vs CNT content for indentation loads of 1, 5, and 10 kg (Figs. 6 a–c, respectively), a decrease in fracture toughness is observed upon addition of 0.01 wt% carbon nanotubes, for both SWCNTs and MWCNTs, this behavior always being more notorious with additions of MWCNTs. For CNT contents higher than 0.01 wt%, the fracture toughness is increased for composites doped with MWCNTs, whereas the general trend is inverse for composites doped with SWCNTs, suggesting enhanced stress transfer capability from the alumina matrix to the MWCNTs for CNT contents above 0.01 wt%, probably due to the improved dispersion of MWCNTs and to a better bond with the Al_2O_3 matrix. When looking at Fig. 6(c), one would prefer to add SWCNTs instead of MWCNTs, but the data might be fooled due to the agglomeration of the SWCNTs with a concomitantly lower reduction of the fracture toughness (see Fig. S2 in Supplementary material). SWCNTs tangle and interact with each other through van der Waals forces, which makes it difficult to obtain a homogeneous dispersion of CNTs in a ceramic powder [47]. Due to their great flexibility and high surface energy, SWCNT tend to aggregate into large bundles with properties generally inferior to those of isolated SWCNT which forms a serious hurdle for real applications [55]. On the other side, in both MWCNT and SWCNT, the toughness of the 0.01 wt% composites is lower than that of the ZTA matrix, due to grain size reduction of the matrix, but increases again up to the level of the ZTA when adding 0.1 wt% CNTs. The grain size reduction of the ZTA matrix is therefore the primary cause for the drop in fracture toughness at 0.01 wt% CNT levels.

On the other hand, the degradation of the fracture toughness in composites with additions of SWCNTs could be primarily attributed to severe agglomeration of the SWCNTs themselves, affecting the load-carrying ability [56]. Compared to other results [47,56–59], describing CNT addition to monolithic alumina, our composites present a more effective improvement of the mechanical properties for CNT contents below 0.5 wt%. The obtained ZTA composite with 0.1 wt% MWCNT additions reached a maximum fracture toughness of 8.17 ± 1.23 MPa $m^{1/2}$ (indentation load of 1 kg) which is statistically comparable to 7.92 ± 0.84 MPa $m^{1/2}$ obtained for the ZTA composite at the same indentation load. This fracture toughness is however higher than reported for pressureless sintered equivalents [43,60]. For a better understanding, Table 3 summarizes the mechanical properties of the composites (diagrams Figs. 4–6). It is well known that the hardness of ceramic composites is usually affected by the intrinsic deformability of the ceramic and microstructural parameters such

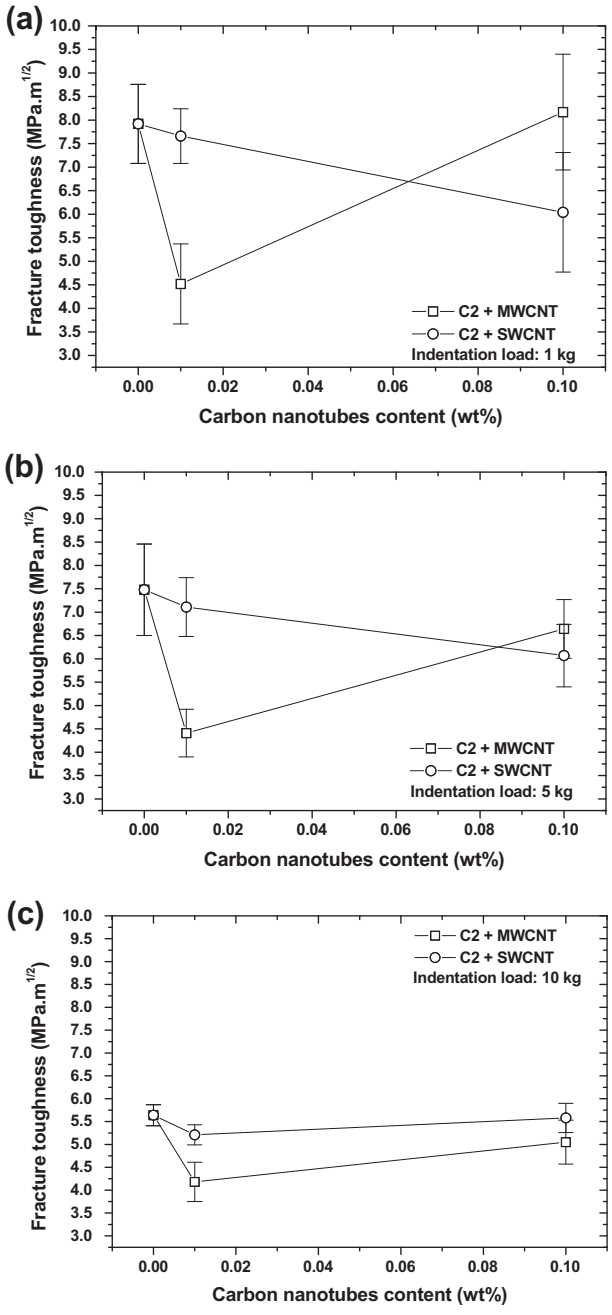

Fig. 6 – Fracture toughness as a function of CNTs (wt%) content (a) indentation load 1 kg, (b) indentation load 5 kg, and (c) indentation load 10 kg.

as multiphases, grain size and orientation, porosity as well as boundary constitution and therefore, the size of the cracks formed under indentation test depends on the nature of the elastic–plastic damage response of the material under indenter limiting in some cases the cracking or even no cracking [61] around the indentation which leads severely to overestimate the fracture toughness when is measured by the standard indentation method according to the pointed out by Wang et al. [23] and Sheldon and Curtin [62]. Although the absolute toughness values obtained by the indentation method might be overestimated, indentation and long crack toughness tests such as the Chevron notch test [53] or the single-edge V-notch beam (SEVNB) technique [63] proved to be able to provide consistent evidence of the toughening role of CNTs. The article by Mazaheri et al. [63] illustrates that for CNT content lower than 0.5 wt% in MWCNT/nanostructured zirconia composites (up to 0.1 wt% CNT content in our study) the calculated fracture toughness for both indentation fracture method and single-edge-V-notched beam one is practically the same. For CNT content higher than this value, the fracture toughness could be overestimated due to the size of the cracks formed under indentation. This appreciation can be supported with the Fig. S3 in Supplementary material for our ZTA composite reinforced with 10 vol% (~5 wt%) of MWCNTs and pressureless sintered [37], where the classical radial cracks in the indentation impression are absent suggesting elastic recovery at the indentation sites, showing a flexibility of nanotube as was reported by Sato et al. [61].

The radial crack (corresponding to the arrow mark in Fig. 7a) of an indented ZTA composite with 0.1 wt% MWCNTs (highest fracture toughness, Fig 6a) is shown in detail in Fig. 7. A predominantly intergranular crack path with a high roughness of the fracture lines/surface is observed, indicating that the crack deflection (zigzag nature) occurred at the grain boundaries being the predominant mechanism for the higher toughness (8.17 ± 1.23 MPa $m^{1/2}$). The ZrO_2 transformation toughening mechanism does not seem to work for these composites taking into account that the small grain size of zirconia particles reduces their ability to transform under applied stress. Generally it is known that toughening mechanisms are directly related to the ZrO_2 grain size and stabilizer content [60]. The very low phase transformation to *m*-ZrO_2 during cooling to room temperature from peak sintering temperature generates few microcracking in the alumina matrix surrounding the zirconia grains as shown in Fig. S4 in Supplementary material. This appreciation has been supported by X-ray diffraction (not shown here). The very limited presence of monoclinic ZrO_2 phase in as-sintered, polished and fractured surfaces, indicates that the contribution of the transformation toughening and microcrack toughening must have been almost irrelevant in the present ZTA composites.

It is assumed that the higher toughness must be a result of the true intergranular fracture in these MWCNTs reinforced ZTA composites [64,65]. Crack bridging (see high magnification inserts of squares in Fig. 7b) was also observed and may contribute as a source of toughening. On the other hand, in the SEM micrographs of a fractured cross-section corresponding to the ZTA/0.01 wt% MWCNTs (see arrow in enlarged square in Fig. 8a) and ZTA/0.1 wt% MWCNTs composites (Fig. 8b), it is observed that MWCNTs were pulled out from the ceramic matrix which in turn could further dissipate fracture energy, this being another possible reason for the additional strengthening and toughening of the ZTA/0.1 wt% MWCNTs by the presence of these MWCNTs [59]. This energy dissipation mechanism can be attributed to the work done by the elastic extension of carbon nanotubes over a distance at either end of the CNTs [45,66].

It is scarce to find MWCNTs in the composite with additions of 0.01 wt% due to their low concentration. The preservation of CNTs after SPS sintering at 1520 °C was confirmed by Raman spectroscopy (see Fig. S5 in Supplementary

Table 3 – Summary of mechanical properties of the experimented composites.

Sample	Hv_1		HV_5		Hv_{10}	
	Vickers hardness (GPa)	Fracture toughness (MPa $m^{1/2}$)	Vickers hardness (GPa)	Fracture toughness (MPa $m^{1/2}$)	Vickers hardness (GPa)	Fracture toughness (MPa $m^{1/2}$)
C2*	20.74 ± 0.28	7.92 ± 0.84	19.28 ± 0.31	7.48 ± 0.98	18.75 ± 0.27	5.64 ± 0.23
C2MW0.1	21.65 ± 0.71	8.17 ± 1.23	20.00 ± 0.19	6.64 ± 0.63	19.39 ± 0.15	5.21 ± 0.22
C2SW0.1	20.27 ± 0.33	6.04 ± 1.27	19.07 ± 0.21	6.07 ± 0.67	18.66 ± 0.17	5.58 ± 0.32
C2MW0.01	20.51 ± 0.45	4.52 ± 0.85	19.73 ± 0.28	4.41 ± 0.51	19.13 ± 0.25	4.18 ± 0.43
C2SW0.01	20.31 ± 0.29	7.66 ± 0.58	19.75 ± 0.16	7.11 ± 0.63	19.54 ± 0.06	5.05 ± 0.48

* C2: 84.975 wt% Al_2O_3 + 0.025 wt% MgO + 13 wt% ZrO_2 (Tosoh 3Y) + 2 wt% $ZrO_{2(m)}$.

material). The typical Raman absorption signals for MWCNTs and SWCNTs appear in their correspondent spectra, taken from fracture surfaces. This result contrasts with the study of Thomson et al. [67] where SWCNT-reinforced alumina composites revealed that the carbon nanotube structure was preserved in Al_2O_3 composites SPSed up to ~1250 °C, whereas it was almost completely broken down after SPS at 1350 °C for only 5 min. The fracture surfaces (hereafter corresponding to samples that were indented with 1 kg of load) of pure ZTA, ZTA reinforced with 0.01 wt% MWCNTs and 0.01 wt% SWCNTs as well as ZTA reinforced with 0.1 wt% MWCNTs and 0.1 wt% SWCNTs composites, are shown in Figs. 9a–e, respectively. From these fracture surfaces, some important features can be observed. For the composite without carbon nanotubes, the fracture is mostly intergranular and characterized by a small number of deviations yet exhibiting large angles and consequently a very tortuous path, explaining the high efficiency of the deflection mechanism and high fracture toughness value (7.92 ± 0.84 MPa $m^{1/2}$). Some MWCNTs were deformed elastically until failure (arrow black and arrow white in Fig. 9b and d, respectively), in a "sword in a sheath" mode (an axial fracture mechanism) where the outer nanotube fractures followed by pullout of the interior walls.

This sword-in-sheath breaking mechanism is a common failure mechanism for MWCNTs loaded in this way [8], which is not present in SWCNTs. On the other hand, the white arrow marks in the insert of Fig. 9b indicate that the diameter of the pullout MWCNT drastically slenderized towards their tip. Axial tensile tests on MWCNTs carried out in an atomic force microscope show that they tend to fracture by a sword-in-sheath mechanism [8]. For fractured nanotubes, a critical

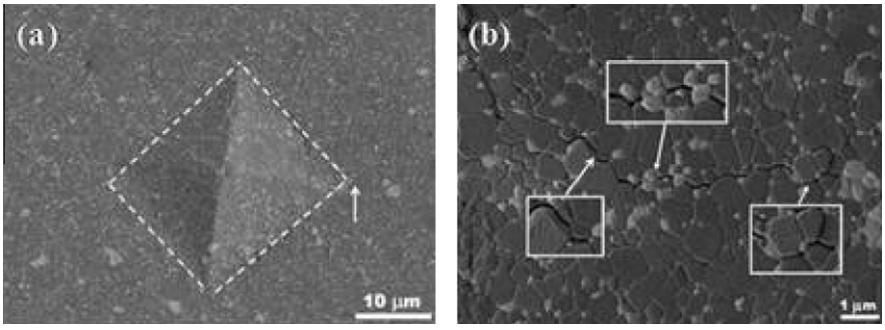

Fig. 7 – SEM micrograph of the polished and thermally etched surface of the ZTA (C2) + 0.1 wt% MWCNs composite showing, (a) the Vickers impression at 1 kg of load, and (b) the arm at higher magnification of the crack marked by an arrow in (a). Squares in (b) are explained in text.

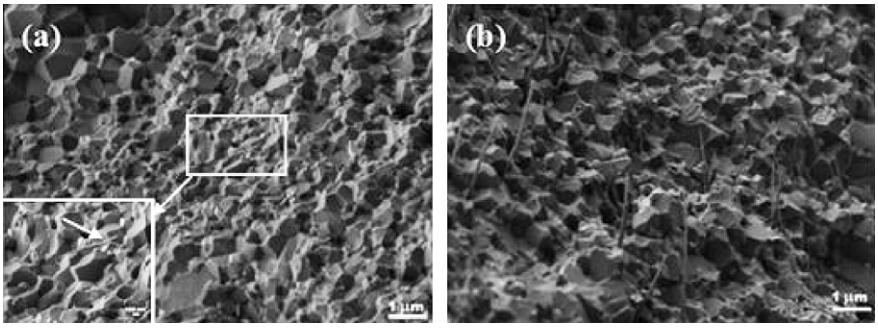

Fig. 8 – Fracture surfaces of the ZTA (C2) composites with additions of (a) 0.01 wt% MWCNTs, and (b) 0.1 wt% MWCNTs.

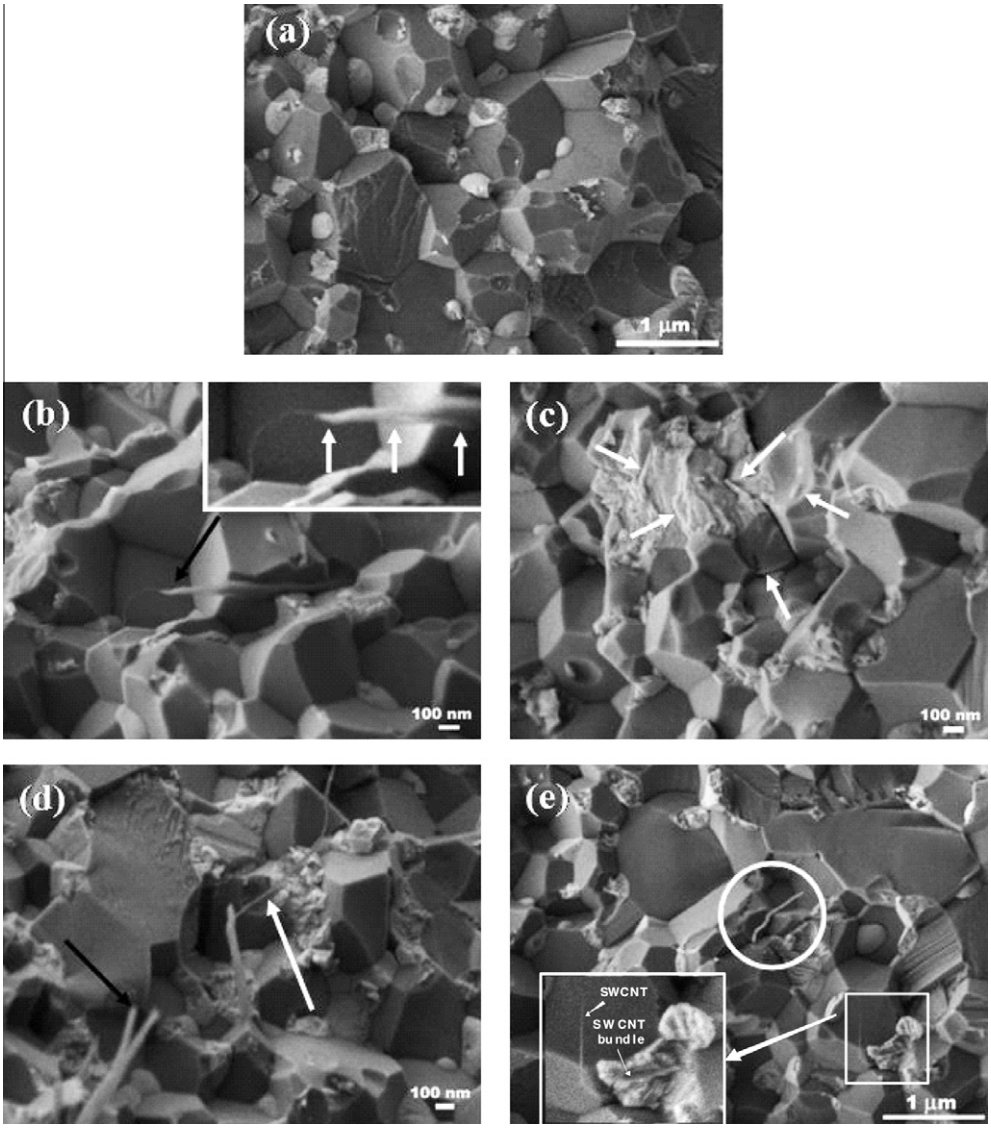

Fig. 9 – SEM of fracture surfaces of as-SPSed (a) pure ZTA (C2), (b) C2 + 0.01 wt% MWCNTs, (c) C2 + 0.01 wt% SWCNTs, (d) C2 + 0.1 wt% MWCNTs, and (e) C2 + 0.1 wt% SWCNTs composites SPSed at 1520 °C. Arrow marks and circle are explained in text.

force is required to pull the fractured wall ends through the outer wall(s). Therefore, a uniformly applied force exercised on the outer MWCNT wall leads to both stick–slip behavior and an increase in the pullout force for fractured nanotubes [68]. Failure of nanotubes by this fracture mechanism suggests good interfacial stress transfer [69].

When a MWCNT axis is nearly perpendicular to the tensile direction, it is believed that it tends to rupture by transversal shear fracture as can be observed in Fig. 9d (CNT identified with black arrow). This observation is consistent with results reported by Qian and Dickey [10]. It is noteworthy that the composite shown in Fig. 9d (ZTA + 0.1 wt% MWCNTs) exhibited the highest fracture toughness of 8.17 ± 1.23 MPa $m^{1/2}$ due to the high deflection angles increasing the tortuosity of the crack path. The microstructures of the ZTA composites reinforced with 0.01 wt% and 0.1 wt% SWCNTs (Fig. 9c and e, respectively) look different, since the SWCNTs are localized mainly parallel to the fracture surface and within the grains (arrow marks in Fig. 9c) implying few pullouts. However, an isolated pullout of SWCNT bundles was observed and the diameter of bundles was observed to decrease toward their tips (arrow marks in enlarged square in Fig. 9e. These results could indicate that the failure in the SWCNTs occurred by intra-bundles sliding due to the weak cohesive bonds between SWCNTs within and between the bundles according to observations by Yamamoto et al. [70] suggesting that the detachment between SWCNTs within and between the bundles is a factor of paramount importance in the fracture process of ceramic composites. The interaction between SWCNTs can be further enhanced by the addition of inter-tube bridging and this method is well described by Kis et al. [71].

Taking into account that the nanotubes in general are randomly dispersed in the alumina matrix, many of them must be bent under severe angles acquiring the shape of the matrix

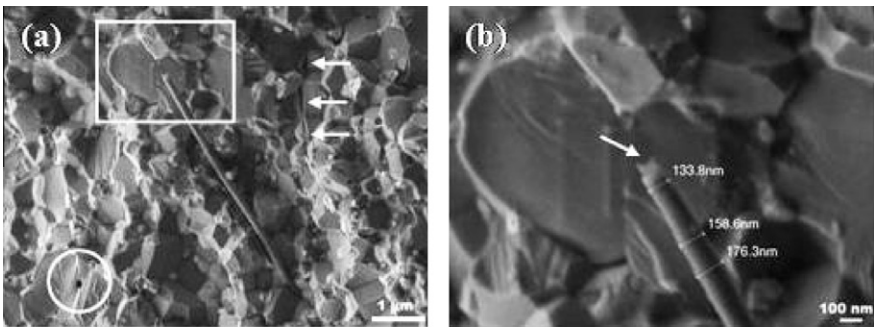

Fig. 10 – SEM of fracture surface of ZTA (C2) composite with additions of 0.1 wt% MWCNTs showing, (a) a broken CNT (square), and (b) higher magnification of the square in (a). Circle in (a) and arrow in (b) are explained in the text. Arrow marks in (a) indicate footprints on the grain boundaries after pull-out of the CNT.

grains at the grain boundary (SWCNT circled in Fig. 9e) and once the CNTs break or are pulled out of the matrix, they elastically spring back to their original conformation. A clear example of this is illustrated in Fig. S6 in Supplementary material, where a multiwall carbon nanotube is observed to debond from the alumina matrix leaving the "footprint" on the fracture surface and subsequently the CNT tends to return to a straight configuration [69], supporting the crack deflection mechanism, which is consistent with the microstructure of Fig. 7b. Fig. 10a shows the alumina matrix attached to a tip of a MWCNT which has been slenderized towards the fractured portion, similar to that observed in broken MWCNTs under tensile load. The different nanotube diameters along the fragment of the carbon nanotube are shown in Fig. 10b, which is a high magnification of the square indicated in Fig. 10a. The arrow in Fig. 10b indicates that the MWCNT was slightly torn which can be attributed to the strong interlayer bonding, indicating an enhancement of effective frictional resistance between individual MWCNTs and the alumina matrix leading to an increase in fracture toughness. The diameter change is clearly shown in Fig. 10b. On the other hand, the hole highlighted by the circle in Fig. 10a could be attributed to a CNT which was completely pulled out from the fracture surface during bridging [72].

In general, the increase in fracture toughness at 0.1 wt% CNT additions could be associated with a suitable adhesion strength of the well-dispersed CNTs to the matrix resulting in a more effective load transfer from the matrix to the CNTs [10]. Comparing the influence of the addition of MWCNTs and SWCNTs on the fracture toughness in ZTA composites, the experimental results reveal that MWCNTs are more effective to toughen ZTA composites prepared by SPS (present work) or conventional pressureless sintering [37]. This observation is in disagreement with the results reported by Sun et al. [73] claiming that the addition of CNTs had a negative influence on the hardness of the composites and no influence on the fracture toughness in 0.1–1.0 wt% MWCNT and SWCNTs/3Y-TZP composites. Compared to pressureless sintered monolithic Al_2O_3 [37], a 244% increase in fracture toughness was realized for the SPSed ZTA composite with 0.1 wt% MWCNTs addition.

4. Conclusions

In this work, relative densities higher than 98% were attained by SPS with and without additions of multi-walled carbon nanotubes (MWCNTs) and SWCNTs. A higher relative density was reached with composites free of CNTs. On the other hand, the Vickers hardness of the ZTA and ZTA-CNT ceramics was found to decrease with increasing indentation load. The higher hardness of the ZTA-CNT composites is attributed to a grain refinement of ZTA matrix. Meanwhile, the fracture toughness also decreases with increasing indentation load. The 10 kg indentation toughness of the ZTA ceramic substantially decreases upon adding 0.01 wt% MWCNTs and SWCNTs, but increases again to the value of the matrix ceramic at 0.1 wt% CNT addition. Due to the grain growth inhibiting effect of the CNTs, the fracture toughness of the ZTA is lowered compared to that of the ZTA ceramic. At higher CNTs content however, the additional toughening mechanisms induced by the nanotubes, i.e. CNT pull-out and crack bridging, restore the original toughness of the matrix. A predominantly intergranular crack path with a high roughness of the fracture lines/surface was observed in the MWCNTs reinforced ZTA composites indicating that the crack deflection (zigzag nature) occurred at the grain boundaries being the more predominant mechanism for higher toughness (8.17 ± 1.23 MPa $m^{1/2}$). Likewise, pull-outs of a small amount of carbon nanotubes and the bridging effect of CNTs during crack propagation, are the other possible mechanisms that contributed to the improvement in fracture toughness. SEM studies provide direct evidence of MWCNTs rupturing in a sword-in-sheath mechanism in the tensile direction suggesting a strong interfacial stress transfer that would equally contribute to a moderate enhancement in fracture toughness. In closing, undoubtedly, the influence of both MWCNTs and SWCNTs on the fracture toughness in ZTA composites is dependent on the dispersion method used, matrix nature, particle size distribution, diameter and length of CNTs. Taking this into account, there is a controversy whether either MWCNTs or SWCNTs are the better reinforcement agents. One should also take into account the Al_2O_3 and ZrO_2 grain size reducing effect of the CNT addition, which has a substantial effect on the mechanical properties of the matrix material

might need to be initially compensated by the additional toughening mechanisms incorporated by the CNT addition.

Acknowledgements

The authors wish to express their appreciation to Wilber Antunez and Joselin Saénz for assistance in SEM. In addition, we would like to thank PhD Verónica González Peña and PhD Maria Elena Llanos Serrano from Instituto Mexicano del Petróleo for Raman spectroscopy studies. K. Vanmeensel thanks the Fund for Scientific Research Flanders (FWO) for his post-doctoral fellowship.

Appendix A. Supplementary data

Supplementary data associated with this article can be found, in the online version, at doi:10.1016/j.carbon.2011.09.031.

REFERENCES

[1] Iijima S. Helical microtubules of graphitic carbon. Nature 1991;354(6348):56–8.
[2] Radushkevich LV, Lukyanovich VM. Carbon structure formed under thermal decomposition of carbon monoxide on iron. Sov J Phys Chem 1952;26:88–95.
[3] Oberlin A, Endo M, Koyana T. Filamentous growth of carbon through benzene decomposition. J Cryst Growth 1976;32(3):335–49.
[4] Abrahamson J, Wiles PG, Rhodes B. Structure of carbon fibers found on carbon arcs anodes. Carbon 1999;37(11):1873–5.
[5] Hirlekar R, Yamagar M, Garse H, Vij M, Kadam V. Carbon nanotubes and its applications: a review. Asian J Pharm Clin Res 2009;2(4):17–27.
[6] Peng B, Locascio M, Zapol P, Li Sh, Mielke SL, Schatz GC, et al. Measurements of near-ultimate strength for multiwalled carbon nanotubes and irradiation-induced crosslinking improvements. Nat Nanotechnol 2008;3(10):626–31.
[7] Barber AH, Andrews R, Schadler LS, Wagner HD. On the tensile strength distribution of multiwalled carbon nanotubes. Appl Phys Lett 2005;87(20). 203106-1-203106-3.
[8] Yu M, Lourie O, Dyer MJ, Moloni K, Kelly TF, Ruoff RS. Strength and breaking mechanism of multiwalled carbon nanotubes under tensile load. Science 2000;287(5453):637–40.
[9] Yamamoto G, Suk JW, An J, Piner RD, Hashida T, Takagi T, et al. The influence of nanoscale defects on the fracture of multi-walled carbon nanotubes under tensile loading. Diamond Relat Mater 2010;19(7-9):748–51.
[10] Qian D, Dickey EC. In-situ transmission electron microscopy studies of polymer-carbon nanotube composite deformation. J Microsc 2001;204(1):39–45.
[11] Cho H, Shi D, Guo Y, Lian J, Ren Z, Poudel B, et al. Enhanced thermal stability of carbon nanotubes by plasma surface modification in Al_2O_3 composites. J Appl Phys 2008;104(7). 074302-1-074302-6.
[12] Ajayan PM, Stephan O, Colliex C, Trauth D. Aligned carbon nanotube arrays formed by cutting a polymer resin-nanotube composite. Science 1994;265(5176):1212–4.
[13] Kuzumaki T, Miyazawa K, Ichinose H, Ito K. Processing of carbon nanotube reinforced aluminium composite. J Mater Res 1998;13(09):2445–9.
[14] Xu CL, Wei BQ, Ma RZ, Liang J, Ma XK. Fabrication of aluminum-carbon nanotube composites and their electrical properties. Carbon 1999;37(5):855–8.
[15] Zhan G-D, Kuntz JD, Wan J, Mukherjee AK. Single-wall carbon nanotubes as attractive toughening agents in alumina-based nanocomposites. Nature 2003;2(1):38–42.
[16] Inam F, Yan H, Peijs T, Reece MJ. The sintering and grain growth behaviour of ceramic-carbon nanotube nanocomposites. Comp Sci Technol 2010;70(6):947–52.
[17] Flahaut E, Peigney A, Laurent Ch, Marliere Ch, Chastel F, Rousset A. Carbon nanotube-metal-oxide nanocomposites: microstructure, electrical conductivity and mechanical properties. Acta Mater 2000;48(14):3803–12.
[18] Zhu Y-F, Shi L, Zhang Ch, Yang X-Z, Liang J. Preparation and properties of alumina composites modified by electric field-induced alignment of carbon nanotubes. Appl Phys A 2007;A89(3):761–7.
[19] Kim SW, Chung WS, Sohn K-S, Son Ch-Y, Lee S. Improvement of wear resistance in alumina matrix composites reinforced with carbon nanotubes. Metal Mater Trans 2010;41A(2):380–8.
[20] Curtin WA, Sheldon BW. CNT-reinforced ceramics and metals. Mater Today 2004;7(11):44–9.
[21] An JW, You DH, Lim DS. Tribological properties of hot-pressed alumina-CNT composites. Wear 2003;255(1-6):677–81.
[22] Siegel RW, Chang SK, Ash BJ, Stone J, Ajayan PM, Doremus RW, et al. Mechanical behavior of polymer and ceramic matrix nanocomposites. Scr Mater 2001;44(8-9):2061–4.
[23] Wang X, Padture NP, Tanaka H. Contact-damage-resistant ceramic/single-wall carbon nanotubes and ceramic/graphite composites. Nature 2004;3(8):539–44.
[24] Pezzotti G, Munisso MC, Porporati AA, Lessnau K. On the role of oxygen vacancies and lattice strain in the tetragonal to monoclinic transformation in alumina/zirconia composites and improved environmental stability. Biomaterials 2010;31(27):6901–8.
[25] Deville S, Chevalier J, Dauvergne CH, Fantozzi G, Bartolome JF, Moya JS, et al. Microstructural investigation of the aging behaviour of (3Y-TZP)-Al_2O_3 composites. J Am Ceram Soc 2005;88(5):1273–80.
[26] Takano Y, Ozawa T, Yoshinaka M, Hirota K, Yamaguchi O. Microstructure and mechanical properties of ZrO_2 (2Y)-toughened Al_2O_3 ceramics fabricated by spark plasma sintering. J Mater Synth Process 1999;7(2):107–11.
[27] Piconi C, Maccauro G, Muratori F, Branch Del Prever E. Alumina and zirconia ceramics in joint replacements. J Appl Biomater Biom 2003;1(1):19–32.
[28] Wang SW, Chen LD, Hirai T. Densification of Al_2O_3 powder using spark plasma sintering. J Mater Res 2000;15(4):982–7.
[29] Shen Z, Johnsson M, Zhao Z, Nygren M. Spark plasma sintering of alumina. J Am Ceram Soc 2002;85(8):1921–7.
[30] Chengtie Wu. Methods of improving mechanical and biomedical properties of Ca-Si based ceramics and scaffolds. Expert Rev Med Devices 2009;6(3):23741.
[31] Shen ZJ, Adolfsson E, Nygren M, Gao L, Kawaoka H, Niihara K. Dense Hydroxyapatite-zirconia composites with high strength for biological applications. Adv Mater 2001;13(3):214–6.
[32] Nygren M, Shen Z. On the preparation of bio-, nano- and structural ceramics and composites by spark plasma sintering. Solid Sci 2003;5(1):125–31.
[33] Zhong H, Wang L, He L, Jiang W, Zhai W, Lin K, et al. Fabrication and characterization of tricalcium silicate bioceramics with high mechanical properties by spark plasma sintering. Int J Appl Ceram Technol 2011;8(3):501–10.
[34] Sarkar SK, Youn M-H, Oh I-H, Lee B-T. Fabrication of CNT-reinforced Hap composites by spark plasma sintering. Mater Sci Forum 2007;534-536:893–6.
[35] Kessel HU, Hennicke J, Kirchner R, Kessel T. Rapid sintering of novel materials by fast/SPS: Further developments to the point of an industrial production process with high cost efficiency. FCT Systeme GmbH. Scientific brochure, 2010.

[36] Orrú R, Licheri R, Locci A, Cincotti A, Cao G. Consolidation/synthesis of materials by electric current activated/assisted sintering. Mater Sci Eng R 2009;63(4-6):127–287.
[37] Bocanegra-Bernal MH, Echeberria J, Ollo J, Garcia-Reyes A, Domínguez-Rios C, Reyes-Rojas A, et al. A comparison of the effects of multi-wall and single-wall carbon nanotube additions on the properties of zirconia toughened alumina composites. Carbon 2011;49(5):1599–607.
[38] Yamamoto G, Shirasu K, Hashida T, Takagi T, Suk JW, An J, et al. Nanotube fracture during the failure of carbon nanotube/alumina composites. Carbon 2011;49(12):3709–16.
[39] Spear RL, Cameron RE. Carbon nanotubes for orthopaedic implants. Int J Mater Forum 2008;1(2):127–33.
[40] Aguilar-Elguézabal A, Antunez W, Alonso G, Paraguay F, Espinosa F, Miki-Yoshida M. Study of carbon nanotubes synthesis by spray pyrolysis and model of growth. Diamond Relat Mater 2006;15(9):1329–35.
[41] ASTM C-1327-99. Standard test method for Vickers indentation hardness of advanced ceramics. Annual Book of ASTM Standards, Vol 14.02, 1999.
[42] Evans AG, Charles EA. Fracture toughness determination by indentation. J Am Ceram Soc 1976;59(7-8):371–2.
[43] Zhou JP, Gong QM, Yuan KY, Wu JJ, Chen Y, Li ChSha, et al. The effect of multiwalled carbon nanotubes on the hot-pressed 3 mol% yttria stabilized zirconia ceramics. Mater Sci Eng A 2009;A520(1-2):153–7.
[44] Peigney A. Tougher ceramics with nanotubes. Nat Mater 2003;2(1):15–6.
[45] Ahmad I, Unwin M, Cao H, Chen H, Zhao H, Kennedy A, et al. Multi-walled carbon nanotubes reinforced Al_2O_3 nanocomposites: mechanical properties and interfacial investigations. Compos Sci Technol 2010;70(8):1199–206.
[46] Chen RZ, Chiu YT, Tuan WH. Toughening alumina with both nickel and zirconia inclusions. J Eur Ceram Soc 2000;20(12):1901–6.
[47] Zhang T, Kumari L, Du GH, Li WZ, Wang QW, Balani K, et al. Mechanical properties of carbon nanotube-alumina nanocomposites synthesized by chemical vapor deposition and spark plasma sintering. Compos Part A 2009;40(1):86–93.
[48] Correa de Sá e Benevides de Moraes MC, Elias CN, Filho JD, Guimaraes de Oliveira L. Mechanical properties of alumina-zirconia composites for ceramic abutments. Mater Res 2004;7(4):643–9.
[49] Krell A. Load dependence of hardness in sintered submicrometer Al_2O_3 and ZrO_2. J Am Ceram Soc 1995;78(5):1417–9.
[50] Celli A, Tucci, Esposito L, Palmonari C. Fractal análisis of cracks in alumina-zirconia composites. J Eur Ceram Soc 2003;23(3):469–79.
[51] Rios CC, Coelho AA, Batista WW, Gonçalves MC, Caram R. ISE and fracture toughness evaluation by Vickers hardness testing o fan Al_3Nb–Nb_2Al–AlNbNi in situ composite. J Alloys Compd 2009;472(1-2):65–70.
[52] Quinn GD, Bradt RC. On the Vickers indentation fracture toughness test. J Am Ceram Soc 2007;90(3):673–80.
[53] Cho J, Inam F, Reece MJ, Chlup Z, Dlouhy I, Shaffer MSP, et al. Carbon nanotubes: do they toughen brittle matrices? J Mater Sci 2011;46(14):4770–9.
[54] Anstis GR, Chantikul P, Lawn BR, Marshall DB. A critical evaluation of indentation techniques for measuring fracture toughness: I, direct crack measurements. J Am Ceram Soc 1981;64(9):533–8.
[55] Coleman J, Khan U, Blau W, Gunko Y. Small but strong: a review of the mechanical properties of carbon nanotube–polymer composites. Carbon 2006;44(9):1624–52.
[56] Yamamoto G, Omori M, Hashida T, Kimura H. A novel structure for carbon nanotube reinforced alumina composites with improved mechanical properties. Nanotechnology 2008;19(31):1–7.
[57] Mo ChB, Cha SI, Kim KT, Lee KH, Hong SH. Fabrication of carbon nanotube reinforced alumina matrix nanocomposite by sol-gel process. Mater Sci Eng 2005;A395(1-2):124–8.
[58] He CN, Tian F, Liu SJ. A carbon naotube/alumina network structure for fabricating alumina matrix composites. J Alloys Compd 2009;478(1-2):816–9.
[59] Zhou JP, Gong QM, Yuan KY, Wu JJ, Chen YF, Li ChS, et al. The effects of multiwalled carbon nanotubes on the hot-pressed 3 mol% yttia stabilized zirconia ceramics. Mater Sci Eng 2009;A520(1-2):153–7.
[60] Echeberria J, Ollo J, Bocanegra-Bernal MH, Garcia-Reyes A, Domínguez-Rios C, Aguilar-Elguézabal A, et al. Sinter and hot isostatic pressing (HIP) of multi-wall carbon nanotubes (MWCNTs) reinforced ZTA nanocomposite: microstructure and fracture toughness. Int J Refract Met H 2010;28(3):399–406.
[61] Sato Y, Ootsubo M, Yamamoto G, Van Lier G, Terrones M, Hashiguchi Sh, et al. Super-Robust, Lightweight, Conducting Carbon Nanotube Blocks Cross-Linked by De-fluorination. ACS Nano 2008;2(2):348–56.
[62] Sheldon BW, Curtin WA. Nanoceramic composites: tough to test. Nat Mater 2004;3(8):505–6.
[63] Mazaheri M, Mari D, Hesabi ZR, Schaller R, Fantozzi G. Multi-walled carbon nanotube/nanostructured zirconia composites: Outstanding mechanical properties in a wide range of temperature. Compos Sci Technol 2011;71(7):939–45.
[64] Ohnishi H, Naka H, Sekino T, Ikuhara Y, Niihara K. Mechanical properties of 2.0–3.5 mol% Y_2O_3-stabilized zirconia polycrystals fabricated by the solid phase mixing and sintering method. J Ceram Soc Jpn 2008;116(12):1270–7.
[65] Muchtar A, Lim LC. Indentation fracture toughness of high purity submicron alumina. Acta Mater 1998;46(5):1683–90.
[66] Maiti K, Sil A. Relationship between fracture toughness characteristics and morphology of sintered Al_2O_3 ceramics. Ceram Int 2010;36(8):2337–44.
[67] Thomson KE, Jiang D, Ritchie RO, Murkherjee AK. A preservation study of carbon nanotubes in alumina-based nanocomposites via Raman spectroscopy and nuclear magnetic resonance. Appl Phys 2007;A89(3):651–4.
[68] Xia Z, Curtin WA. Pullout forced and friction in multiwall carbon nanotubes. Phys Rev B 2004;69(23). 233408-1-233408-4.
[69] Estili M, Kawasaki A, Sakamoto H, Mekuchi Y, Kuno M, Tsukada T. The homogeneous dispersión of surfactantless, slightly disordered, crystalline, multiwalled carbon nanotubes in α-alumina ceramics for structural reinforcement. Acta Mater 2008;56(15):4070–9.
[70] Yamamoto G, Sato Y, Takahashi T, Omori M, Tohji K, Hashida T. Mechanical properties of Single-Walled Carbon nanotube Solids Prepared by Spark Plasma Sintering. J Solid Mechan Mater Eng 2007;1(7):854863.
[71] Kis A, Csányi G, Salvetat J-P, Lee T-N, Couteau E, Kulik AJ, et al. Reinforcement of single-walled carbon nanotube bundles by intertube bridging. Nature 2004;3(3):153–7.
[72] Ahmad I, Cao H, Chen H, Zhao H, Kennedy A, Zhu YQ. Carbon nanotube toughened aluminium oxide nanocomposite. J Eur ceram Soc 2010;30(4):865–73.
[73] Sun J, Gao L, Iwasa M, Nakayama T, Niihara K. Failure investigation of carbon nanotube/3Y-TZP nanocomposites. Ceram Int 2005;31(8):1131–4.